







Article

Cobalt Based Catalysts on Alkali-Activated Zeolite Foams for N₂O Decomposition

Zdeněk Tišler ¹, Anna Klegová ², Eliška Svobodová ^{1,*}, Jan Šafář ¹, Kateřina Strejcová ¹, Jan Kohout ¹, Stanislav Šlang ³, Kateřina Pacultová ², Daily Rodríguez-Padrón ⁴ and Roman Bulánek ⁵

¹ Unipetrol Centre for Research and Education, a.s, Areál Chempark 2838, Záluží 1, 436 70 Litvínov, Czech Republic; zdenek.tisler@unicre.cz (Z.T.); jan.safar@unicre.cz (J.Š.); katerina.strejcovova@unicre.cz (K.S.); jan.kohout@unicre.cz (J.K.)

² Institute of Environmental Technology, VSB-Technical University of Ostrava, 17. listopadu 15/2172, 708 00 Ostrava, Czech Republic; anna.klegova@gmail.com (A.K.); katerina.pacultova@vsb.cz (K.P.)

³ Center of Materials and Nanotechnologies, Faculty of Chemical Technology, University of Pardubice Nam. Cs. Legii, 530 02 Pardubice, Czech Republic; stanislav.slang@upce.cz

⁴ Departamento de Química Orgánica, Campus de Rabanales, Universidad de Córdoba, Edificio Marie Curie (C-3), Ctra Nnal IV-A, Km 396, E14014 Cordoba, Spain; dailydggs@gmail.com

⁵ Department of Physical Chemistry, Faculty of Chemical Technology, University Pardubice, Studentská 573, 532 10 Pardubice, Czech Republic; roman.bulanek@upce.cz

* Correspondence: eliska.svobodova@unicre.cz

Received: 16 October 2020; Accepted: 27 November 2020; Published: 30 November 2020



Abstract: In this work, we studied the effect of alkali-activated zeolite foams modifications on properties and catalytic activity of cobalt phases in the process of catalytic decomposition of N₂O. The zeolite foam supports were prepared by alkali activation of natural zeolite followed by acid leaching and ion exchange. The cobalt catalysts were synthesised by a different deposition technique (direct ion exchange (DIE) and incipient wetness impregnation (IWI) method of cobalt on zeolite foams. For comparison, catalysts on selected supports were prepared and the properties of all were compared in catalytic tests in the pellet form and as crushed catalysts to determine the effect of internal diffusion. The catalysts and supports were in detail characterized by a variety of techniques. The catalyst activity strongly depended on the structure of support and synthesis procedure of a cobalt catalyst. Ion exchange method provided active phase with higher surface areas and sites with better reducibility, both of these factors contributed to higher N₂O conversions of more than 80% at 450 °C. A large influence can also be attributed to the presence of alkali metals, in particular, potassium, which resulted in a modification of electronic and acid base properties of the cobalt oxide phase on the catalyst surface. The promotional effect of potassium is better reducibility of cobalt species.

Keywords: natural zeolite; clinoptilolite; zeolite foam; alkali activation; cobalt catalyst; N₂O decomposition

1. Introduction

The alkali-activated materials have properties very similar to zeolites but do not form crystalline structures. These materials can be prepared by activating a variety of aluminosilicate components. Raw materials for the preparation of these materials, e.g., natural zeolites, most often occur as compact fine-grained rocks formed by sedimentary or volcanic activity, whose main component is zeolite clinoptilolite, belonging to the group of heulandite, accompanied by minerals from the group of feldspars, clays and mica. Due to their properties, natural zeolites are widely used as sorbents for water purification (Cs⁺, Rb⁺ and NH₄⁺) or gases (NH₃) [1,2]. They do not have suitable properties for use in catalysis, which requires their modification by processes such as dealumination [3,4], desilication or

ion exchange [5]. These modifications improve the properties in the desired direction, e.g., increase the specific surface area or reduce the content of accompanying elements (Fe, K, Na, Ca and Mg). The same modification procedures can be used to modify the properties of zeolite foams which, in addition to almost any desired shape (pellets, blocks, crumb) and macroporosity not present in the original zeolite material, impart the desired properties of the zeolite material. Macroporosity is advantageous not only for diffusion reasons but also for structural reasons, as this material reduces weight of catalyst/sorption bed and thus the complexity of the equipment and its robustness requirements [6].

Alkali-activation of natural zeolite produces a foam material consisting of the original zeolite (clinoptilolite) structure and the N/K-A-S-H binder matrix ($\text{Na}_2\text{O}/\text{K}_2\text{O}-\text{Al}_2\text{O}_3-\text{SiO}_2-\text{H}_2\text{O}$) that binds the individual grains of aluminosilicate component. This binder matrix is formed by the reaction of the alkaline activator with an aluminosilicate (natural zeolite). These materials with the additional macroporous structure are prepared by alkaline activation of natural zeolite with a mixed activator based on potassium hydroxide and sodium silicate. The macroporous structure is obtained by foaming an activated mixture of metal powders (Al, Mg, Zn) [6–8], solutions containing hydrogen peroxide [8,9], silica fume or silicon powder [10,11]. Subsequent reaction of these components with the alkaline activator results in the evolution of a gas which foams the activated mixture.

The foaming of the alkali-activated mixture and following post-synthesis modification of prepared materials e.g., by acid leaching create a well permeable foam structure of low density in which micro-, meso- and macropores are present. Acid leaching is often used for post-synthesis modification of zeolites to remove framework aluminium and, in the case of alkali-activated materials, other accompanying elements (K, Na, Ca, Fe, Mg), presented in the basic zeolite grains or binder matrix. This leaching of the material creates additional porosity, which is important for the easier permeability of foams [8]. The second option for post-synthesis modification of foams is the ion exchange (IE). This method is widely used for zeolites and due to the similarity of alkali-activated materials, this technique can also be used for the removing of Na and K ions or exchanging another cation [8].

Nitrous oxide (N_2O) is considered as an important pollutant contributing to the greenhouse effect even though it is not the major contributor. However, unlike the main contributors (CO_2 and CH_4), it is much more efficient greenhouse gas [12]. The largest industrial sources of N_2O emissions are waste gases from nitric acid production plants in a global amount of more than 400 kt of N_2O per year [12]. Catalytic decomposition of N_2O can be performed directly in the NH_3 burner (temperature around 900 °C, catalysts based on oxides, spinels and perovskite materials) or behind the burner, when the gas temperature is only 250–500 °C. In addition to the possibility of thermal decomposition of N_2O (by increasing the gas temperature to 750–1000 °C), non-selective or selective catalytic reduction of N_2O (requiring the addition of reducing agents such as hydrogen, natural gas, LPG, NH_3 , etc.) is the most economically advantageous direct catalytic decomposition of N_2O . The low-temperature catalytic decomposition of N_2O (up to 450 °C) to nitrogen and oxygen offers an attractive way to decrease N_2O emissions in tail gas from nitric acid production plants. Results from a number of catalytic systems have been published. For example, catalysts based on transition metals (Cu, Co, Ni, Fe) or catalysts based on precious metals (Rh, Ru, Pd) using various catalyst supports (ZnO, CeO_2 , Al_2O_3 , TiO_2 , ZrO_2 , zeolites, hydrotalcites and perovskites). This study is focused on cobalt-based catalysts that show excellent catalytic activities at low temperature (≤ 450 °C) in the decomposition of N_2O [12–30].

Catalysts based on synthetic zeolites are successfully used and studied in a number of catalytic applications including catalytic decomposition of nitrous oxide. Synthetic cobalt modified zeolites (Beta, Y, ZSM-5, etc.) [31], eventually modified by other metals like iron or copper [32], were often studied. These catalysts show very good results in the catalytic decomposition of N_2O , conversions reach up to 100% at 425 °C and given experimental conditions [33]. The disadvantage in comparison with natural zeolites and materials formed therefrom, for example, alkali-activated foams, is in particular that their synthesis is relatively time-consuming and economically demanding. On the other hand, the use of leached modified natural zeolite with subsequent ion exchange (IE) encounters some limitations, such as unsatisfactory textural properties or limited IE capacity [34].

In addition to zeolite catalysts, other types of catalysts prepared, for example, by impregnation of other supports, precipitated catalysts or catalysts prepared by other techniques based on the presence of spinel phases of cobalt or mixed Co-Mn-Al phases are studied for catalytic N_2O decomposition [11,24,27,35]. Modification of the cobalt spinels with a small amount of alkali metals significantly increases the activity of the catalyst, alkali metal promoter lowers the work function of the cobalt spinel facilitating redox processes that occur between the catalyst surface and the reaction oxygen intermediates produced during the N_2O decomposition leading to the significant increase in the catalytic activity [14,17,23,27,35–38]. Synthesis conditions of the Co spinel oxide could significantly affect catalytic properties. Different methods were described for the preparation of cobalt oxide-based catalysts: (co)-precipitation from cobalt nitrate solution using different precipitation agents like Na_2CO_3 [20,39], K_2CO_3 [40,41], $(NH_4)_2CO_3$ [16], KOH [42] and $NH_3 \cdot H_2O$, NaOH [39], by thermal treatment of cobalt nitrate [24,43,44], cobalt carbonate [14,24] or cobalt benzoate-dihydrazinate complex [45] and by solution combustion synthesis from cobalt nitrate and urea [43]. Equally, the deposition of active phase on suitable support has a significant impact. Therefore, the selection of suitable support could lead to more efficient utilization of active phase. It is achieved by applying a thin active layer to the support material. Supported cobalt oxide N_2O catalysts were studied mainly on different monoliths [46–49], sieves [32,50], tablets, pellets or extrudates [29,51] and ceramic foams [52].

The work aims to prepare cobalt catalysts based on alkali-activated zeolite foams and determine the influence of catalyst support modifications and cobalt oxide loading method on physic-chemical properties and catalytic activity in N_2O decomposition. Acid leaching and ion exchange of alkali activated zeolite foam (AZF) were used to prepare catalyst supports, which were subsequently impregnated with cobalt nitrate, and after annealing, cobalt oxide catalysts were obtained. The same method was used to prepare comparative catalysts using alumina as a support. The effect of different preparation on the properties of the active phase was studied on catalysts prepared by direct ion exchange (DIE) of basic alkali activated zeolite foam, as well as the promotional effect of manganese in Co catalyst in catalytic decomposition of N_2O . The effect of Mn, was monitored in our study because CoMnAl HTC 4:1:1 catalysts are often reported to have very good results. Studied catalytic materials showed significant differences in the textural properties and chemical composition of the active phase resulting in significant differences in activity depending on the chosen modification method. All catalysts were characterized by various instrumental techniques and tested in the N_2O catalytic decomposition in inert gas. The obtained results showed the further possible use of catalysts based on alkali-activated zeolite foams in catalytic applications. In the field of industrial catalysis, in addition to the catalytic results, the ease of synthesis, affordability and the price of the catalysts used are also important, and therefore, these materials have a lot to offer.

2. Results and Discussion

2.1. Characterisation of the Catalysts and Supports

Zeolite foam used as catalyst support was prepared by foaming of alkali-activated natural zeolite mixture. Obtained porous solid foam material was post-synthesis modified (i) by acid leaching with 3M HCl or (ii) by ion-exchange treatment using 1M NH_4NO_3 .

As-prepared zeolite foam (AA-S, Table 1) had a higher alkali metals content than natural zeolites due to the use of mixed alkaline activator KOH + Na_2SiO_3 . Chemical composition of Al_2O_3 can be seen in Appendix A Table A1. A part of the alkaline activator occurred in a form of mixed Na/K silicate, which can be seen in images from SEM equipped with EDS analyser as a leaf-like particles (Figure 1). Ion-exchange treatment of AA-S sample using NH_4NO_3 solution (AA-N) reduced predominantly content of K and Na cations. A part of K^+ and Na^+ ions was in “unchangeable positions” trapped inside of the zeolite and/or other aluminosilicates framework [4,8]. Results of chemical composition analysis (Table 1) showed a noticeable effect of HCl leaching (AA-D). HCl mostly reduced the alkali

content (K, Na) in addition to other elements (Fe, Ca, Mg and especially Al), which resulted into higher Si/Al ratio (up to 11.8 from the original 5.8).

Table 1. Chemical composition and specific surface area of catalysts and zeolite foam supports.

Sample	Chemical Composition (wt.%)								Si/Al Ratio (mol/mol)	Co/AM * Ratio	SSA ** (m ² /g)
	Si	Al	K	Na	Ca	Fe	Co	Mn			
AA-S	33.4	5.5	7.2	2.9	2.3	0.9	-	-	5.8	-	15.0
AA-N	37.8	6.3	1.6	0.3	1.7	1.1	-	-	5.8	-	23.4
AA-D	42.0	3.4	1.1	0.2	0.5	0.7	-	-	11.8	-	111.7
AA-S-Co	30.5	5.1	6.6	2.6	2.1	0.9	6.4	-	5.7	0.4	13.5
AA-N-Co	35.0	6.0	1.4	0.2	1.6	1.0	5.7	-	5.6	2.1	27.7
AA-D-Co	38.7	3.5	1.1	0.2	0.4	0.7	5.4	-	10.6	2.5	49.9
AA-IE-Co	32.0	5.2	4.1	0.5	1.7	0.9	6.3	-	5.9	0.9	115.8
AA-IE-CoMn	31.9	5.2	4.2	0.5	1.7	0.9	5.4	0.8	5.9	0.7	118.6

* AM = alkali metals (Na + K), ** SSA = specific surface area (BET).

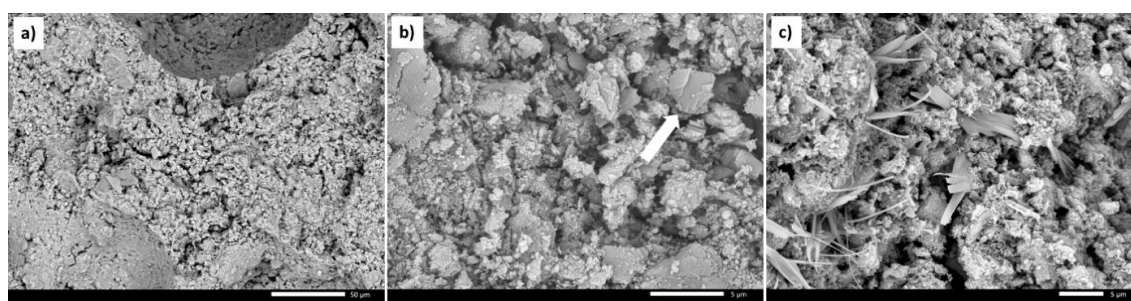


Figure 1. Macroporous structure of zeolite foam AA-S (a), crystalline Na/K silicate (white arrow) in AA-S (b) and leaves of Na/K silicates in AA-S-Co catalyst (c).

These three types of support based on zeolite foams (AA-S, AA-N, AA-D) and one commercial supports (γ -Al₂O₃) were used to prepare cobalt catalysts with 5 wt.% Co content. The actual cobalt content ranged from 4.8 to 6.4 wt.%, as determined by XRF the slightly higher cobalt content was due to the non-stoichiometric water content of the cobalt nitrate hydrate. The last two catalysts tested (AA-IE-Co and AA-IE-CoMn) were prepared by a direct ion-exchange method using a solution of cobalt nitrate, and mixture of cobalt nitrate with manganese nitrate, respectively. The cobalt content of AA-IE-Co catalysts was 6.3 wt.% and the cobalt content of the AA-IE-CoMn catalyst was 5.4 wt.% and manganese 0.8 wt.%, respectively. The cobalt content was average for the whole pellet, so the cobalt content in the active layer of AA-IE-Co catalyst is higher than 6.3 wt.% (theoretically up to about 13 wt.% or about up 11 wt.% for AA-IE-CoMn catalyst). The molar ratio of Co/Mn is 6.5:1, the difference compared to the target ratio (Co/Mn 4:1) is due to the different course of precipitation of Co and Mn ions during the formation of the layer in the pellet. Catalysts prepared using this method had a significantly higher content of potassium and slightly higher content of sodium in comparison with a catalyst impregnated on AA-N support. This showed that cobalt precipitation precluded complete ion-exchange of Na⁺ and K⁺ ions by Co²⁺ ion. Higher Na and K contents were observed only for the AA-S-Co catalyst, but the alkalis were present here in the form of Na/K silicates. As Table 1 shows, the presence of these components had a very negative effect on the specific surface area (SSA) because the silicates closed the pores. Additionally, due to pore opening and cleaning, there was also an increase in specific surface area (SSA) two times for (AA-N) and more than seven times for AA-D. SSA of catalysts did not change significantly compare to original supports. The decrease of SSA was observed only for alumina and AA-D supported catalyst, which could have been caused by partially blocking the pores with cobalt, more precisely, its oxide. This decrease in AA-D was related to blockade of clinoptilolite micropores which have been released by acid leaching [4,8]. The catalysts

AA-IE-Co and AA-IE-CoMn prepared in this way exhibit relatively high specific surface (SSA) areas compared to catalysts employing differently modified zeolite foam supports (Table 1). This was probably partially caused by the formation of porous cobalt and cobalt-manganese oxides originating from precipitated hydroxides on the zeolite foam surface, or by partial cleaning of the zeolite foam surface (an increase of crystallinity or intensity respectively was observed, Figure 2) and accessibility of pores. The increase in the surface area has not yet been satisfactorily explained but has been verified by repeated measurements. Rutkowska [53] states that the increase in surface area of the samples (Cu, Fe and Co beta zeolites) could be related to the secondary recrystallization of zeolites during the preparation of catalysts. In this case, it could also be caused by changes in the binder N/K-A-S-H phase or by the generation of additional porosity between the cobalt and manganese hydroxides deposited on the sample surface.

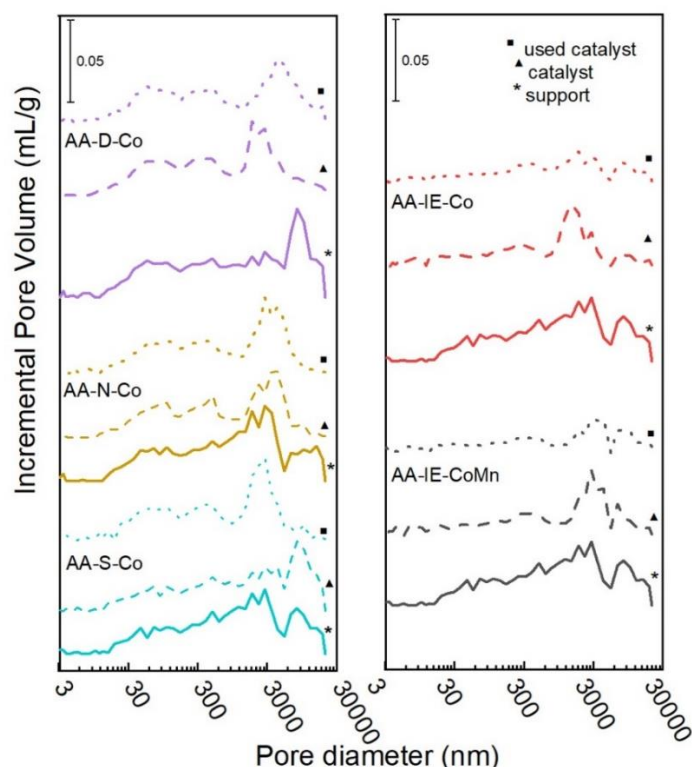


Figure 2. Pore distribution of supports, fresh and used cobalt catalysts.

Since the samples are predominantly macroporous materials, textures of catalytic supports and prepared catalysts were determined via Hg porosimetry. The obtained results (Figure 2) showed that other supports contain predominantly bigger pores. Zeolite foams have broad pore spectrum from mesopores to macropores to supermacropores with a diameter of tenths to hundreds of micrometres with corresponding pore mean size thousands nm. Total intrusion volume of zeolite foams varies from 0.65 (AA-S) to 0.75 mL/g (AA-D). Intrusion volume of their “mesopores” is from 0.06 mL/g (AA-S), 0.07 mL/g (AA-N) to 0.09 mL/g (AA-D). Increase in total intrusion volume and share of AA-D support mesopores was caused by cleansing the surface from the excess alkali activator and mineral sediments inside the pores of natural zeolite. In the case of cobalt catalysts as well of used catalysts (after catalytic reaction of N₂O decomposition), there were no big changes (decreases) observed in intrusion volume. Changes were only due to blocking the pores with cobalt oxide. In contrast, an increase of the mesopore volume was observed in AA-IE-Co and AA-IE-CoMn catalysts (both 0.09 mL/g), which can be attributed to cobalt oxides formed during the catalyst synthesis. Alumina as comparative support is purely mesoporous material with the overall intrusion volume of 0.5 mL/g and mean pore diameter

5.6 nm, Co-Al₂O₃ catalyst shows a partial reduction in intrusion volume due to cobalt oxides deposited on the surface (Appendix A Figure A1).

SEM-EDS mapping of catalyst pellet cross-section (Figure 3) showed identical macroporous structure of the catalysts (every first figure in the row) and homogeneous distribution of cobalt on the surface of the modified zeolite foam catalyst support in the case of AA-N-Co and AA-D-Co catalysts (Figure 3b,c). In case of impregnation of the AA-S support (Figure 3a), an area non-covered by cobalt was observable in the middle of the pellet, which could be caused by precipitation of cobalt hydroxide during impregnation process by alkali agents in the zeolite foam. This as-created layer was blocking further impregnation inside the pellet. Certainly, this will also be affected by the inhomogeneity of the pellets caused by the synthesis method used. A similar effect was observed during preparations via the direct ion-exchange method. As can be seen in Figure 3d,e cobalt was observed only on the outer surface of the pellet in the form of a ring. The depth of cobalt penetration reached approximately 0.7 mm. The difference in depth compared to AA-S-Co was due to different catalyst preparation conditions (solution concentration, temperature, etc.). Manganese distribution showed a decline in content from the surface to the core, but in comparison with cobalt, there was not a strong borderline. There was a significant decline in content of sodium and potassium (observable from grey and yellow colour intensity on Figure 3) in the following order: AA-S-Co, AA-IE-Co/AA-IE-CoMn, AA-N-Co and AA-D-Co and distribution in the whole cross-section is in agreement with results of chemical analysis (XRF).

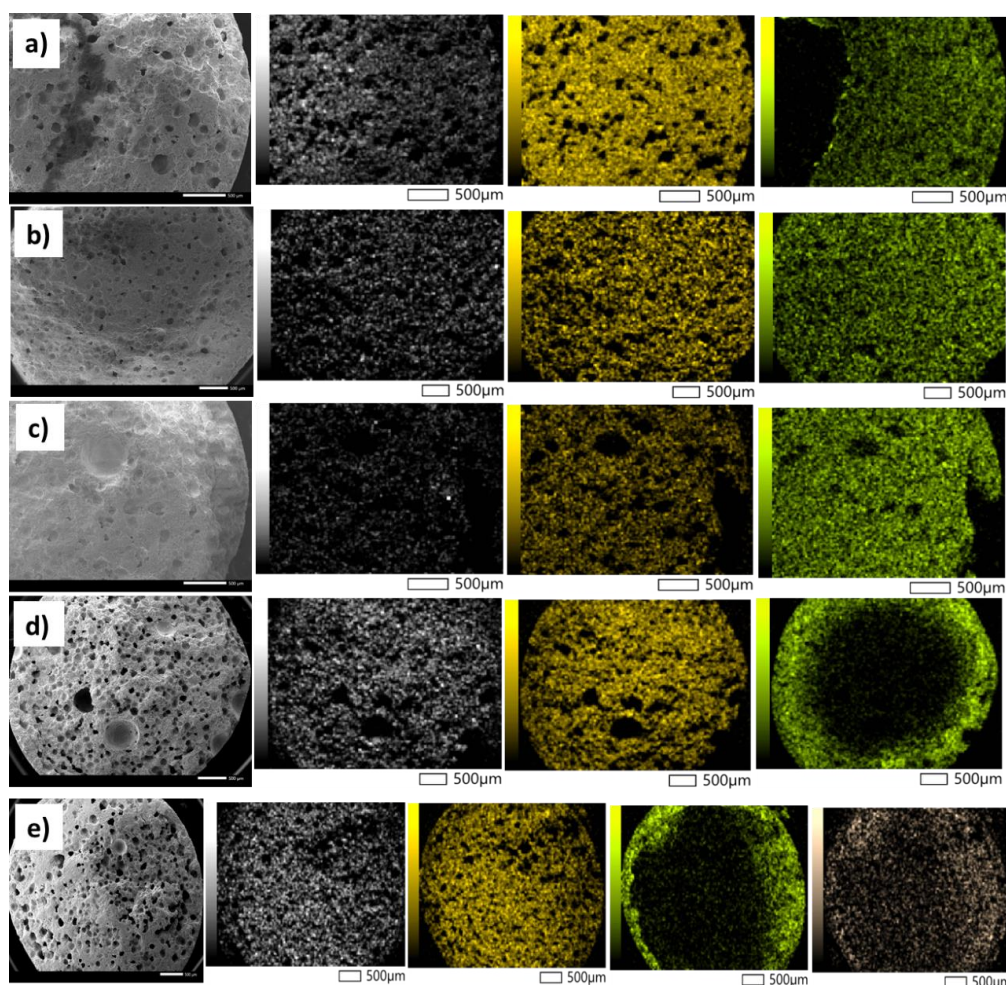


Figure 3. SEM-EDS elemental mapping of sodium (gray), potassium (yellow), cobalt (green) and manganese (brown) on cross section of AA-S-Co (a), AA-N-Co (b), AA-D-Co (c), AA-IE-Co (d) and AA-IE-CoMn (e) catalysts.

The crystalline structure of materials was determined using X-ray powder diffraction (XRD). In case of zeolite foam supported catalysts, the analysis showed clinoptilolite to be a main crystalline phase with typical reflections at 2θ 9.9°, 11.2°, 17.5° and 22.4° (PDF 83-1261) along with other minor phases in the natural zeolite, belonging to the mineralogic group of clays and feldspars (Figure 4a). The diffractograms showed the difference in crystallinity or intensities of main reflections of clinoptilolite respectively depending on the modification method used. The crystallinity of alkali-activated material was lower in comparison with the original natural zeolite [8]. This may be caused by a partial structure disruption during the alkaline activation. There was a significant increase in crystallinity after IE using NH_4NO_3 caused by surface cleansing. In contrast, after leaching with 3M HCl, there was a decrease in crystallinity connected with disruption of the zeolite structure due to removing Al from the clinoptilolite crystalline matrix. During the modification process, there was a change in intensities at 2θ 11.2°/9.9° that corresponded to planes (020) and (200), caused by the difference in electron density in that plane. From the original ratio 0.5 in the natural zeolite, the value increases after alkali-activation to 0.8 and after leaching with HCl or IE treatment, it decreases to 0.4 [8]. Comparative catalysts showed typical broad reflections for $\gamma\text{-Al}_2\text{O}_3$ (2θ 46.5° and 67.3°, PDF 74-2206) (Appendix A Figure A2).

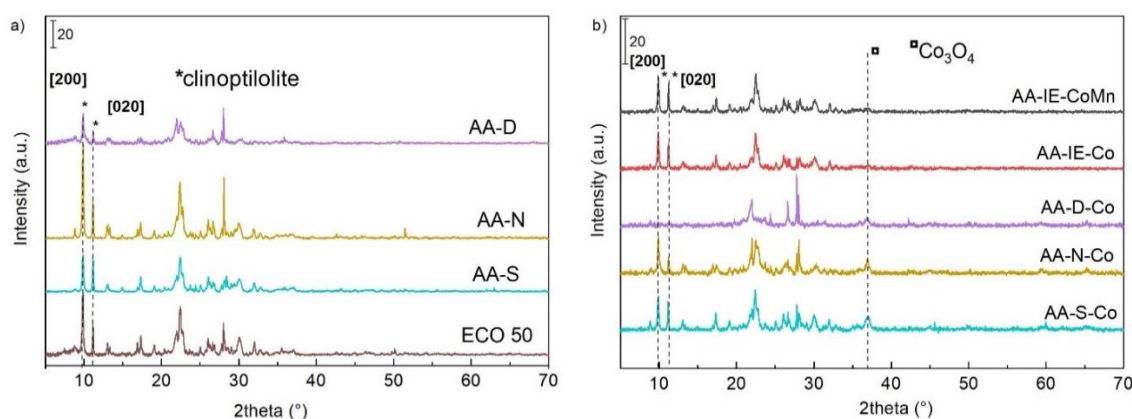


Figure 4. Powder diffraction patterns of supports (a) and fresh catalysts (b).

Cobalt catalysts prepared using these supports showed significant crystalline structures corresponding to Co_3O_4 (2θ 31.5°, 36.9°, 45.0°, 55.7°, 59.6° and 65.6°, PDF 65-3103). These were the most apparent in case of using alumina as support (Appendix A Figure A2). In case of other supports (Figure 4b), there was only one reflection visible (36.9° 2θ), while AA-D supported catalysts showed the reflections corresponding to clinoptilolite (2θ 9.9° and 11.2°) and other minor phases (clays and feldspars) with no significant intensities corresponding to cobalt oxide. This indicated homogeneous distribution of cobalt on the surface without the formation of a crystalline Co_3O_4 phase. Crystallite size of Co_3O_4 calculated using the Scherrer equation from the reflection 36.9° 2θ is 12 nm for catalysts with alumina support. It was not possible to evaluate the crystallite size in other catalysts due to overlap of cobalt oxide diffraction with line assigned to the clinoptilolite, quartz or anorthite.

Analysis of the used catalysts (Appendix A Figure A3), samples labelled with additional -U, catalysts after their usage for N_2O decomposition test) did not show any significant changes in the crystalline structure compared with fresh catalysts. Powder diffraction patterns of Al_2O_3 can be seen in Appendix A Figure A2. After using the catalysts in the reaction test only slight decreases in intensity are noticeable. Only in the case of the AA-D-Co-U catalyst, there was a significant decrease in intensities 2θ 27.8°, 28.0° and others corresponding to anorthite (PDF 71-0748).

Temperature-programmed ammonia desorption (NH_3 -TPD) showed significant differences in the amount and strength of acid sites (Figure 5a) of each catalyst (Table 2). While the catalyst supported on industrial support (Al_2O_3 -Co) showed low acidity (Appendix A Table A2, Figure A4a), the zeolite foam supported catalysts showed changes in acidity depending on the support modification method during catalyst preparation. In general, peaks at low temperatures, below 200 °C are attributed to weakly

acidic sites or physisorbed ammonia, and peaks at higher temperatures in the range of 200–400 °C are associated with the interaction of NH₃ with acidic Brønsted sites attributed to strongly acidic sites. Peaks at temperatures above 400 °C correspond to the interaction of NH₃ with Lewis acids and are attributed to Co-O species that form very strongly acidic sites [54–56]

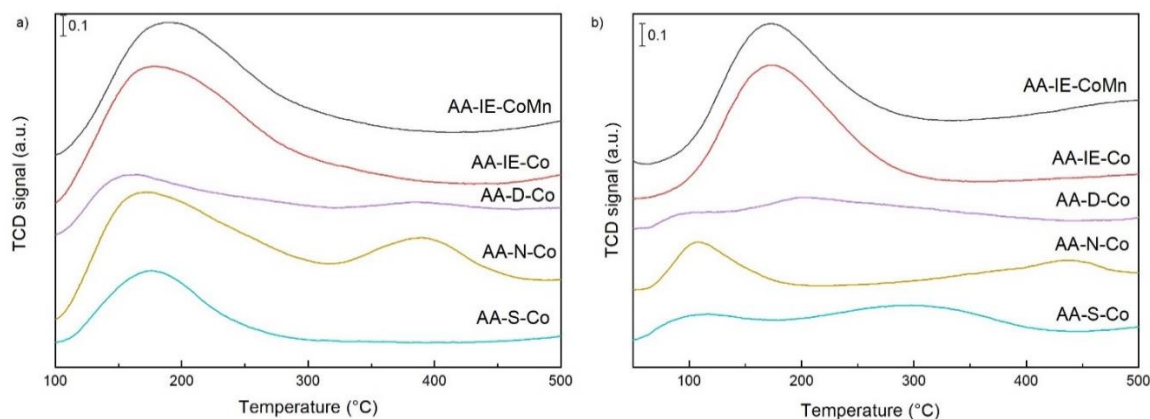


Figure 5. Acidity (a) and basicity (b) of cobalt catalysts determined by NH₃-TPD and CO₂-TPD, respectively.

Table 2. Acidity of cobalt catalysts determined by ammonia TPD.

Sample	c _{SUM} (μmol/g)	T _{max1} (°C)	c _{max1} (μmol/g)	P _{max1} [*] (%)	T _{max2} (°C)	c _{max2} (μmol/g)	P _{max2} [*] (%)	T _{max3} (°C)	c _{max3} (μmol/g)	P _{max3} [*] (%)
AA-S-Co	501	175	501	100	-	-	-	-	-	-
AA-N-Co	1542	173	1313	85	390	229	15	-	-	-
AA-D-Co	593	158	446	75	255	70	12	382	77	13
AA-IE-Co	1446	178	1379	95	247	27	2	362	40	3
AA-IE-MnCo	1211	187	1211	100	-	-	-	-	-	-

* P = population of the relevant sites, index 1–first deconvolution peak, 2–second deconvolution peak and 3–third deconvolution peak.

The highest total acidity exhibited catalyst prepared via impregnation of ion-exchange modified support (AA-N-Co), which contained a high population of strong acid sites, i.e., sites with high NH₃ desorption temperature. The acidity of AA-S-Co and AA-D-Co catalysts is about one-third in comparison and very similar to each other, which is probably due to poor availability of acid sites in the base zeolite–clinoptilolite for AA-S-Co and in case of AA-D-Co due to acid centre removal during acid leaching. Samples prepared using direct ion-exchange treatment showed slightly lower acidity than AA-N-Co, but no strong acid sites.

The basicity of the catalysts was determined by temperature programmed desorption of CO₂ (CO₂-TPD). The data obtained (Table 3, Figure 5b) showed significant low temperature peaks around 110 °C for ion-exchange treated (AA-N-Co) catalyst, direct ion-exchange treated (AA-IE-Co and AA-IE-CoMn) catalysts and a similar maximum is also observed for the Al₂O₃-Co catalyst (Appendix A Table A3, Figure A4b). The basicity is related to the alkali content, i.e., alkali metals (Na + K) in the sample (Table 3). The AA-S-Co catalyst had the highest alkali content, but a large part of the alkali metals was inaccessible to the interaction (they were enclosed in the binder N(A)-A-S-H phase), while in the case of AA-IE-Co and AA-IE-CoMn catalysts which had also higher SSA, alkali metals were more available and the samples showed high overall basicity, especially also the content of weakly basic sites. On the other hand, the basicity of the samples may also be related to the adsorption of CO₂ on the polar adsorption centres, i.e., on all coordination unsaturated cations present in the sample.

Table 3. Basicity of cobalt catalysts determined by CO₂-TPD.

Sample	c _{SUM} (μmol/g)	T _{max1} (°C)	c _{max1} (μmol/g)	P _{max1} * (%)	T _{max2} (°C)	c _{max2} (μmol/g)	P _{max2} * (%)	T _{max3} (°C)	c _{max3} (μmol/g)	P _{max3} * (%)
AA-S-Co	213	105	42	20	186	161	76	321	10	14
AA-N-Co	125	110	82	66	363	14	11	437	30	23
AA-D-Co	156	112	36	23	204	44	28	289	76	49
AA-IE-Co	306	111	215	70	338	91	30	-	-	-
AA-IE-MnCo	408	113	227	56	273	181	44	-	-	-

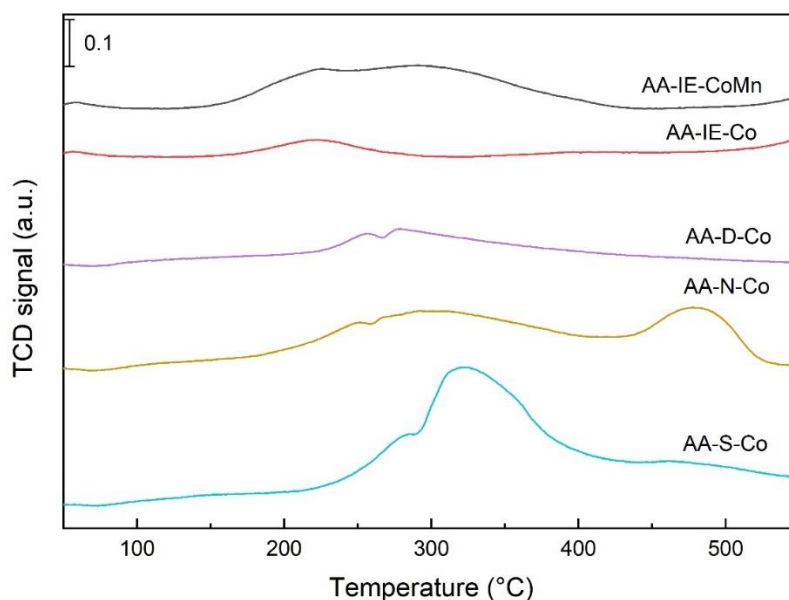
* P = population of the relevant sites, index 1–first deconvolution peak, 2–second deconvolution peak and 3–third deconvolution peak.

The results of the H₂-TPR analysis performed on the catalyst pellets show significant differences in H₂ consumption (Table 4), which corresponds to the content of various forms of Co oxides present on the surface of the catalyst support. Co₃O₄ reduction takes place in two steps, most often parameters for reduction of Co³⁺ to Co²⁺ are the temperature range of 250–300 °C and higher than 400 °C for reduction of Co²⁺ to Co⁰ [9,10]. From the obtained TPR profiles (Figure 6) it can be seen that the reduction took place in the two steps, but significant differences are observed for the individual catalysts. The results of the H₂-TPR analysis performed on the Al₂O₃ can be seen in Appendix A Table A4 and Figure A5.

Table 4. Reducibility of cobalt catalysts determined by TPR.

Sample	c _{SUM} (μmol/g)	T _{max1} (°C)	c _{max1} (μmol/g)	P _{max1} * (%)	T _{max2} (°C)	c _{max2} (μmol/g)	P _{max2} * (%)	T _{max3} (°C)	c _{max3} (μmol/g)	P _{max3} * (%)
AA-S-Co	360	289	77	21	330	218	61	478	65	19
AA-N-Co	875	304	704	80	483	171	20	-	-	-
AA-D-Co	260	284	76	29	306	184	71	-	-	-
AA-IE-Co	176	222	60	34	418	116	66	-	-	-
AA-IE-MnCo	500	239	337	67	303	163	33	-	-	-

* P = population of the relevant sites, index 1–first deconvolution peak, 2–second deconvolution peak and 3–third deconvolution peak.

**Figure 6.** H₂-TPR profiles of cobalt catalysts.

The shift of the reduction peaks may occur due to (i) the presence of alkali [35] which generally lowers temperatures of reduction of cobalt species, or (ii) due to the interaction between the Co₃O₄ spin phase and the support used [51]. In case of the alumina supported catalyst, only one wide reduction peak was evident with two maxima at 435 °C and 479 °C, indicating cobalt species interaction with Al₂O₃ to form Co aluminates with stronger oxygen bonds that decrease reducibility (Appendix A Table A4, Figure A5) [11]. The catalyst using the AA-S basic support exhibited a wide reduction peak

associated with the interaction of Co_3O_4 with alkali (Na/K), the high content of which comes from the excess alkali activator. AA-N-Co and AA-D-Co catalysts had a wide reduction band at about 300 °C, which in the case of AA-N-Co was accompanied by a second reduction band at a maximum of 483 °C corresponding to the less reducible Co species (bulk Co_3O_4) [1]. The shift of reduction peaks towards the lower temperatures of AA-IE-Co and AA-IE-CoMn catalysts was caused by a different catalyst synthesis process, during which Co and CoMn hydroxides and consequently different cobalt species ($\text{CoO}(\text{OH})$) were created on the support surface than in the IWI method [2]. These catalysts also contained a relatively high potassium content, which also significantly lowers the cobalt particle reduction temperature. The second maximum for the AA-IE-CoMn catalyst at 303 °C was related to the interaction of Co with Mn and the reduction of manganese (Mn^{4+} to Mn^{3+}), which was reduced at about 300 °C [3]. TPR profiles showed that deposition of Co_3O_4 on various supports significantly affects the reducibility, i.e., the strength of the binding of Co^{3+} and Co^{2+} to oxygen.

2.2. N_2O Catalytic Decomposition

The prepared cobalt catalysts were tested in laboratory units under defined conditions. The temperature dependence of N_2O conversions using pelletized catalysts are shown in Figure 7a. The results showed significant differences in activity between catalysts due to different properties (chemical composition, textural and acid-base properties, reducibility). The catalyst prepared on a commercial Al_2O_3 support (Al_2O_3 -Co) exhibited very low N_2O conversion (only 7% at 450 °C) (Appendix A Figure A6), even though it had the highest specific surface area of all catalysts tested. As shown by H_2 -TPR, the low catalytic activity was due to the formation of hardly reducible species which cannot participate in N_2O decomposition. The conversion of N_2O on cobalt catalysts supported on differently modified zeolite foams increased in following order: AA-D-Co \rightarrow AA-S-Co \rightarrow AA-N-Co with N_2O conversions at 450 °C of 29%, 43% and 81% respectively. The order of zeolite foamed catalysts correlates with data obtained from TPR. Based on NH_3 -TPD analysis it can be observed that the activity was probably also influenced by the presence of acid centres, which in case of AA-N-Co was the highest of all catalysts tested, followed by AA-IE-Co and AA-IE-CoMn, whose activity at N_2O decomposition was also high (conversion at 450 °C 63% and 79%, respectively). As Obalová et al. have shown, the influence of acidic and basic sites usually begins to apply only when measured under process conditions, which is in the presence of NO and H_2O . For the decomposition of N_2O on oxides, acidic and basic centres are generally not considered important [56]. Samples AA-IE-Co and AA-IE-CoMn show a relatively large effect of the manganese promoter on N_2O decomposition (conversion at 450 °C increases from 63% to 79%). These catalysts contain a cobalt or cobalt-manganese phase in the form of hydroxides and a relatively high content of alkalis, especially potassium, which have a beneficial effect on N_2O decomposition due to better reducibility of cobalt or cobalt-manganese species, as has also been demonstrated using catalysts based on mixed Co-Mn-Al phases doped by alkaline and prepared from hydrotalcite-like precursors [11,24,27,35].

The different shape of the conversion curves of the AA-S-Co catalyst showed a possible textural effect that has been verified via catalytic tests carried out in a small laboratory reactor using a crushed catalyst at a fraction of 160–315 μm . The order of N_2O conversions of the catalysts obtained using the pellets (Figure 7a) and the crushed catalysts (Figure 7b) was different, indicating that the reaction kinetics were influenced by the textural properties of the catalysts and the internal diffusion had a significant effect.

N_2O conversion under the same reaction conditions was used to calculate reaction rates. Assuming that the rate of reaction on the crushed catalyst was not affected by internal diffusion, it can be used to compare the effect of diffusion in pellets [51]. The kinetic constant k ($\text{m}^3\text{s}^{-1}\text{kg}^{-1}$) for pellets and crushed catalyst was calculated from the conversion of N_2O ($X_{\text{N}_2\text{O}}$) at 450 °C, according to the relation (1):

$$k = \ln\left(\frac{1}{1 - X_{\text{N}_2\text{O}}}\right) / \frac{m}{V} \quad (1)$$

where m (kg) is the mass of the active phase in the pellet or crushed catalyst and \dot{V} (m^3s^{-1}) is the total gas flow. The $k_{\text{pellet}}/k_{\text{grain}}$ ratio calculated from experimental data indicates the effect of internal diffusion. This ratio was only 0.12 for the AA-S-Co catalyst, indicating a significant internal diffusion effect. In contrast, catalysts on modified foamed supports basis AA-N-Co ($k_{\text{pellet}}/k_{\text{grain}}$ ratio = 0.99), AA-D-Co ($k_{\text{pellet}}/k_{\text{grain}}$ ratio = 1.06) showed that the effect of internal diffusion was very small or virtually none. The method of preparation of the AA-S-Co catalyst does not make it possible to eliminate these diffusion effects by changing the synthesis procedure. This can be achieved by further post-synthesis modification of the prepared alkali-activated zeolite foam by ion exchange and acid leaching. Although the AA-S-Co catalyst shows the best results for temperatures up to 350 °C, the AA-N-Co catalyst is the best for applications, followed by the AA-D-Co catalyst, even though they are less active in the kinetic mode. This confirms that it is not enough for the active catalyst to have only an effective active phase, but also the structural and textural properties, which are manifested only in shaped samples. The Al_2O_3 -Co catalyst showed no activity under the selected conditions and therefore it was not possible to determine the effect of internal diffusion. As shown on SEM-EDX, another possible explanation may be the inhomogeneity in terms of the distribution of cobalt and potassium in the pellet. For some samples (e.g., AA-S-Co) the results may be skewed because after grinding only a small amount is used (the composition of the catalyst for pellet and powder tests may therefore differ).

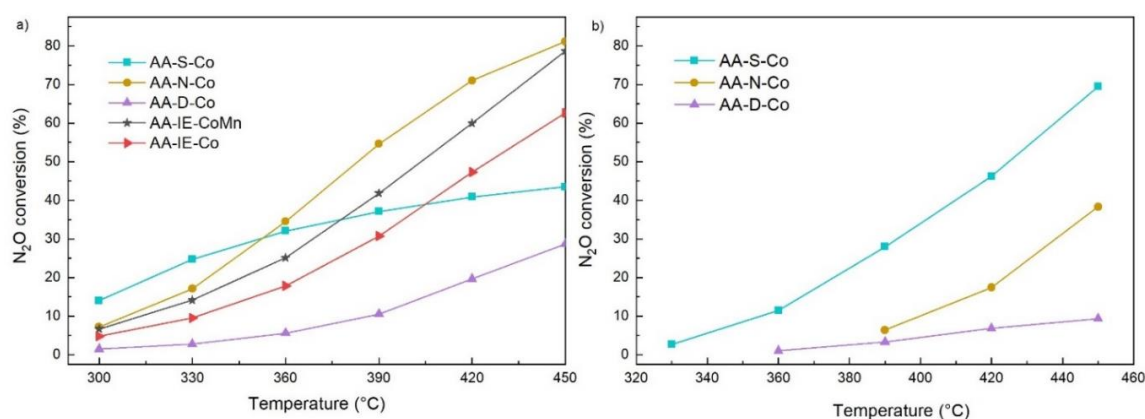


Figure 7. N₂O conversions over pellets of catalysts at GHSV of 3000 m³ m_{bed}⁻³ h⁻¹ (5.1 m³ kg⁻¹ h⁻¹ for AA-S-Co, 5.8 m³ kg⁻¹ h⁻¹ for AA-N-Co and 6.1 m³ kg⁻¹ h⁻¹ for AA-D-Co) (a) and crushed catalyst at GHSV 20 m³ kg⁻¹ h⁻¹ (b).

To compare and explain the differences in catalytic activities of pellets and powders, the rate constants for the individual catalysts and temperatures were calculated and then linearized using Arrhenius Equation (2):

$$k = Ae^{\frac{E_A}{RT}} \rightarrow \ln k = \ln A - \frac{E_A}{RT} \quad (2)$$

where $y = a + bx$ the individual components of the equation correspond to the general regression line: $\ln k = y$, $\ln A = a$, $-(E_A/T) = b$ a $1/T = x$, R is gas constant ($\text{J mol}^{-1}\text{K}^{-1}$), A is pre-exponential factor and T is the temperature (K) [39]. From the values thus obtained, activation energies (E_A) of N₂O decomposition for individual catalysts were determined (Table 5). N₂O is a stable molecule and decomposes only at high temperatures (above 1000 °C), the activation energy of thermal decomposition of N₂O is about 250 kJ/mol [5]. Due to the catalyst, the decomposition temperature or E_A (Table 5) drops very significantly and when using cobalt catalysts based on alkali-activated zeolite foams, it ranges from $\frac{1}{3}$ to $\frac{1}{4}$ of this value (in a range of 60.7–87.3 kJ/mol). Catalysts AA-D-Co, AA-IE-CoMn and AA-IE-Co have E_A very similar with a value of about 70 kJ/mol.

Table 5. Kinetic parameters for N₂O decomposition over cobalt based catalysts in the pellet and crushed form.

Sample	k_{390} ($\text{m}^3 \text{s}^{-1} \text{kg}^{-1}$)	k_{390}^* ($\text{m}^3 \text{s}^{-1} \text{m}^{-2}$)	E_A (J mol^{-1})	E_A^*/E_A
AA-S-Co	6.59×10^{-4}	4.88×10^{-2}	60,750	2.29
AA-N-Co	1.27×10^{-3}	4.58×10^{-2}	87,322	1.52
AA-D-Co	1.89×10^{-4}	3.80×10^{-3}	74,589	1.77
AA-S-Co *	1.82×10^{-3}	1.35×10^{-1}	139,135	-
AA-N-Co *	3.65×10^{-4}	1.32×10^{-2}	132,484	-
AA-D-Co *	1.84×10^{-4}	3.69×10^{-3}	131,677	-
AA-IE-Co	5.97×10^{-4}	5.15×10^{-3}	69,927	-
AA-IE-MnCo	8.75×10^{-4}	7.38×10^{-3}	71,050	-

* crushed catalyst.

The ratio of activation energies of pellets and crushed catalysts (Table 5), which is in the range of 1.5 to 2.3 indicates that the effect of internal diffusion is dominant even in the case of the AA-S-Co catalyst, where the effectiveness factor was only 0.12. The obtained data confirmed our original assumption that the catalysts operate in the kinetic region and this discrepancy is rather due to the inhomogeneity of the sample in terms of the distribution of cobalt and potassium in the pellet. The inhomogeneity of the pellet and the small weight of catalyst used for the crushed catalyst tests led to skewed results.

The results obtained on cobalt catalysts using zeolite foam as support (AA-N-Co, AA-IE-Co, AA-IE-CoMn) are comparable to the results presented on other types of catalysts, e.g., CoMnAl mixed oxide catalysts prepared from a hydrotalcite precursor are very efficient and show similar results under the same conditions, but as other authors have shown in their studies of catalysts, other parameters such as Co/Mn ratio or type and content of alkalis (Na, K, Cs) need to be sensitively optimized [11,27]. In different studies, the same authors also dealt with catalysts using foam or ceramic supports.

The synthesized AA-IE-Co and AA-IE-CoMn catalysts prepared on zeolite foam have significantly higher N₂O conversion (3×–4× higher at temperatures up to 390 °C and 2× higher at temperatures 420–450 °C) in comparison with catalysts prepared on SiC foams with an active layer consisting of CoMnAl mixed oxide (hydrotalcite precursor, Co content about 6 wt.%), under the same conditions [43].

Likewise, the cobalt phase on a cordierite monolith provided with a washcoat layer of CeO₂-ZrO₂ showed about 2× lower conversion of N₂O even though the Co content in the catalyst was almost doubled (13.5 wt.%) [49]. Similar results as AA-IE-Co (under the same test conditions) were shown by a cobalt catalyst prepared by repeated impregnation of a MgO/Al₂O₃ support. Again, however, this catalyst had a significantly higher Co content (25 wt.%) [51]. Cobalt catalysts on beta zeolite (2 wt.% of Co) showed slightly better results under similar conditions, which is due to the better distribution of Co on the surface, as these catalysts have 4 to 6 times higher specific surface area (500–750 m²/g) [52].

Catalytic tests show that the active phase on a support with a high specific surface area (γ -Al₂O₃) may not be the most advantageous solution due to the presence of poorly reducible cobalt species. A suitable alternative may be macroporous foam supports based on alkali-activated natural zeolites with suitable post-synthesis modification or a suitable process of catalyst synthesis. Advantage of these materials was also their ease of synthesis and low cost, meeting the industry's requirements for later large-scale application. In further research, it will be possible to increase the catalytic activity of the cobalt-based active phase applied to the foam support by other promoters such as caesium or by adding other elements such as manganese and cerium. It will be important to optimize their amount and, last but not least, to optimize the actual production processes of the zeolite foam to obtain an optimal distribution of the active phase on its surface. Subsequent long-term testing of the most active catalysts will, in addition to the stability of the catalyst, also monitor the process of deactivation and eventual reactivation of the catalyst and with the contribution of advanced analytical techniques such as X-Ray Photoelectron Spectroscopy (XPS), Transmission Electron Microscopy (TEM) or Auger

Electron Spectroscopy (AES), it will be possible to characterize Co species in detail on the catalyst surface and elucidate reaction and deactivation mechanisms.

3. Materials and Methods

3.1. Materials

Analytical grade potassium hydroxide, hydrogen peroxide (30 wt.%), hydrochloric acid (35 wt.%), ammonium nitrate and cobalt hexahydrate nitrate were supplied by Lach-Ner s.r.o. Sodium silicate (silicate modulus 3.22) was purchased from Labar s.r.o. in a technical grade purity, the powdered natural zeolite ECO 50 (ZEOCEM[®], Slovakia) and γ -Al₂O₃ (2.5 mm spheres, Sasol, Germany) were used.

ZeoCem Eco 50 contains at least 85 wt.% of clinoptilolite and minor mineral components: clays, feldspar, mica. The chemical composition and specific surface areas are shown in Table 6.

Table 6. Chemical composition and specific surface area.

Sample	Chemical Composition (wt.%)								Si/Al Ratio (mol/mol)	SSA * (m ² /g)
	Si	Al	K	Fe	Ca	Na	Mg	Ti		
ECO 50	35.2	6.7	3.5	1.3	3.1	0.2	0.5	0.1	5.2	26.4
γ -Al ₂ O ₃	0.1	51.8	-	-	-	0.4	0.3	-	-	309.0

* BET specific surface area measured by N₂ physisorption.

3.2. Synthesis of Zeolite Foams

Zeolite foam pellets were obtained by the same procedure described in our previous publication [8]. Natural zeolite ECO 50 was activated with a mixed alkaline activator (KOH solution with a sodium silicate) and foamed by hydrogen peroxide solution. Mixture parameters are shown in Table 7. Shaped foam pellets (5 mm diameter) were activated for 48 h at 50 °C. Prepared pellets were aged under laboratory conditions in a closed plastic bag for 1 month prior to further processing. A prepared sample of alkali-activated zeolite foam (AZF) is designated “AA-S”.

Table 7. Alkali-activated mixture parameters.

Parameter	Value
Silicate modulus of the alkaline activator	M _s = 1.51
Water coefficient:	w = 0.7
Alkali content	Me ₂ O * = 8.2 wt. %
Alkali molar ratio	Na ₂ O:K ₂ O = 0.56

* Me = K + Na.

3.3. Post-Synthesis Modifications and Catalyst Synthesis

The foam pellets AA-S were first dried overnight at 120 °C, then, part of them was leached at 80 °C using 3M HCl for 6 h (AA-D). The second part of pellets was ion-exchanged by 1M solution of NH₄NO₃ at 80 °C for 6 h (AA-N). The foam to solution ratio (g/mL) was 1:20 for both modified supports. The cobalt catalysts were synthesized by IWI method with aqueous cobalt nitrate solution on target cobalt content of 5 wt.% (AA-S-Co, AA-N-Co and AA-D-Co). The comparative Al₂O₃-Co catalyst using γ -Al₂O₃ as catalyst support was prepared by the same methods. Other catalyst samples were synthesized by DIE method of AA-S pellets at 80 °C (6 hrs) by 0.25 M solution of cobalt nitrate (AA-IE-Co) or by 0.2 M cobalt nitrate with 0.05 M manganese nitrate respectively (AA-IE-CoMn). All samples (IWI + DIE) were dried overnight at 120 °C and calcined at 500 °C for 4 hrs (1 °C/min). An overview of prepared catalysts is given in Table 8.

Table 8. Prepared catalysts overview.

Catalyst	Support	Preparation Method
Al ₂ O ₃ -Co	Commercial (γ -Al ₂ O ₃)	IWI
AA-S-Co	AZF (AA-S)	IWI
AA-N-Co	Ion exchanged AZF (AA-N)	IWI
AA-D-Co	Acid leached AZF (AA-D)	IWI
AA-IE-Co	AZF (AA-S)	DIE
AA-IE-CoMn	AZF (AA-S)	DIE

3.4. Characterisation of Supports and Prepared Catalysts

Materials in form of pellets were used for all methods except the XRD.

The X-ray diffraction patterns (XRD) were evaluated by D8 Advance ECO (Bruker AXS GmbH, Karlsruhe, Germany) instrument applying CuK α radiation ($\lambda = 1.5406 \text{ \AA}$) with the resolution of 0.02° in the 2θ range of $5\text{--}70^\circ$. The diffractograms were evaluated using the Diffrac.Eva software with the Powder Diffraction File database (PDF 4 + 2018, International Centre for Diffraction Data). The chemical composition of supports and catalysts was determined by X-ray fluorescence analysis (XRF) of powder materials using an S8 Tiger (Bruker AXS GmbH, Karlsruhe, Germany) with Rh cathode.

The N₂ physisorption and Hg porosimetry (MIP) were used for textural properties determination. Prior to the analysis, all samples were dried under vacuum in a glass-cell at 110°C (200°C for calcined materials) for 16 h. The specific surface area was determined from N₂ sorption isotherms at -196°C , measured by Autosorb iQ (Quantachrome Instruments, Boynton Beach, FL, USA). Meso and macroporous properties of catalysts and supports were determined by MIP measurements performed on the AutoPore IV 9510 Hg porosimeter (Micromeritics Instrument Corporation, Norcross, GA, USA). The samples were prepared for the analyses in the same way as for the physisorption measurements.

For scanning electron microscopy (SEM) analysis, samples were coated with about 5 nm of gold to make them conductive under the microscope (JEOL JSM-IT500HR, Tokyo, Japan) accessorized with energy-dispersive X-ray spectroscopy (EDS) for elemental analysis and map analysis. Representative backscattered electron or secondary electron images of microstructures were taken in high vacuum mode using an accelerating voltage of 15 kV.

The reducibility of the cobalt species in the catalysts was determined by H₂-TPR using an AutoChem 2950 HP (Micromeritics Instrument Corporation, Norcross, GA, USA) instrument. The pellets of the sample in a quartz U-tube were heated in He flow at 450°C before the measurement. The reduction was carried out at $t = 40\text{--}500^\circ\text{C}$ with a temperature ramp of $10^\circ\text{C}/\text{minute}$ under reducing gas flow (10 vol.% H₂ in Ar). The changes in hydrogen concentration were monitored by a TCD detector. Acid properties of the samples were characterized by NH₃ and CO₂ temperature-programmed desorption (NH₃-TPD or CO₂-TPD) using the same instrument as for TPR. Prior to TPD experiment, the sample was pre-treated by heating to 450°C (heating rate $10^\circ\text{C}/\text{min}$; kept at target temperature for 30 min) in the flow of He (flow rate 25 mL/min). After reaching 450°C , the sample was cooled down to 100°C (NH₃-TPD) or 50°C (CO₂-TPD). Then, the sample was saturated with NH₃ or CO₂ by flowing the sample bed by a gas mixture containing 90 vol.% of He and 10 vol.% of NH₃ or CO₂ (flow rate 25 mL/min) for 30 min. Weakly bonded NH₃ or CO₂ molecules were removed by flushing the sample out under flow of helium (25 mL/min) for 15 min. Finally, NH₃-TPD experiment was carried out by increasing the temperature from 100 to 500°C (CO₂-TPD of the temperature from 50 to 500°C) with heating rate $10^\circ\text{C}/\text{min}$. The desorbed NH₃/CO₂ in the outlet gas was detected by TCD detector. The obtained curves were evaluated by deconvolution using a SW device.

3.5. Catalytic Tests

Catalytic decomposition of N₂O was performed in integral stainless-steel fixed bed reactor at the temperature range from 300 to 450°C and at atmospheric pressure. The feed introduced to the reactor contained 0.1 mol % N₂O in N₂ and IR analyser (Sick) was used for N₂O analysis. Testing of the grained

catalysts was performed in a reactor with an internal diameter of 5.5 mm and shaped catalysts (foam and pellets) were tested in a reactor with an internal diameter of 50 mm. Grained catalyst bed contained 0.3 g of sample with a particle size of 160–315 μm and 100 mL/min, GHSV of 20 $\text{m}^3\text{kg}^{-1}\text{h}^{-1}$ were used. Pelleted catalyst bed contained 20 mL of sample and 1000 mL/min, GHSV of 3 000 $\text{m}^3\text{m}_{\text{bed}}^{-3}\text{h}^{-1}$ were used. According to different bulk densities of the samples GHSV of 3 000 $\text{m}^3\text{m}_{\text{bed}}^{-3}\text{h}^{-1}$ resulted in different values expressed as $\text{m}^3\text{kg}^{-1}\text{h}^{-1}$ (5.1 $\text{m}^3\text{kg}^{-1}\text{h}^{-1}$ for AA-S-Co, 5.8 $\text{m}^3\text{kg}^{-1}\text{h}^{-1}$ for AA-N-Co and 6.1 $\text{m}^3\text{kg}^{-1}\text{h}^{-1}$ for AA-D-Co).

4. Conclusions

Cobalt catalysts prepared by various techniques on alkali-activated zeolite foams have been characterized in detail and tested in catalytic decomposition of N_2O . For comparison, catalyst was prepared on commercial $\gamma\text{-Al}_2\text{O}_3$ support with identical content of cobalt phase (5 wt.%). Tests were also performed on crushed catalysts to determine the effect of internal diffusion. Despite the significantly higher specific surface area of the catalyst on $\gamma\text{-Al}_2\text{O}_3$ support, catalysts on zeolite foams had significantly higher N_2O conversions. The reason is that hardly reducible cobalt phases were formed on $\gamma\text{-Al}_2\text{O}_3$, while the zeolite foams did not have such a strong internal diffusion effect and besides, due to the presence of alkali, especially potassium, the cobalt phase had better N_2O decomposition properties. Manganese doping of the cobalt catalyst further improved the catalyst properties and the N_2O conversion increased by 25%. The results obtained show the great potential of these catalysts on alkali-activated zeolite foams in general and move them closer to further use in industrial applications.

Author Contributions: Conceptualization, Z.T. and E.S.; methodology, Z.T.; validation, A.K., J.Š. and R.B.; formal analysis, E.S.; investigation, Z.T., K.S., J.K., K.P., D.R.-P.; resources, A.K., S.Š., K.P.; data curation, K.S., J.K.; writing—original draft preparation, Z.T. and E.S.; writing—review and editing, Z.T., K.S., R.B., A.K., K.P.; visualization, E.S.; supervision, Z.T. All authors have read and agreed to the published version of the manuscript.

Funding: This publication is a result of the project CATAMARAN, Reg. No. CZ.02.1.01/0.0/0.0/16_013/0001801, which has been co-financed by European Union from the European Regional Development Fund through the Operational Programme Research, Development and Education. This project has also been financially supported by the Ministry of Industry and Trade of the Czech Republic which has been providing institutional support for long-term conceptual development of research organization. The project CATAMARAN has been integrated into the National Sustainability Programme I of the Ministry of Education, Youth and Sports of the Czech Republic (MEYS) through the project Development of the UniCRE Centre (LO1606). The result was achieved using the infrastructure of the project Efficient Use of Energy Resources Using Catalytic Processes (LM2018119) which has been financially supported by MEYS within the targeted support of large infrastructures. Experimental results were accomplished by using Large Research Infrastructure ENREGAT supported by the Ministry of Education, Youth and Sports of the Czech Republic under project No. LM2018098. Authors appreciate financial support from grants LM2018103 from the Ministry of Education, Youth and Sports of the Czech Republic.

Conflicts of Interest: The authors declare no conflict of interest. The funders had no role in the design of the study; in the collection, analyses, or interpretation of data; in the writing of the manuscript, or in the decision to publish the results.

Appendix A

Table A1. Chemical composition and specific surface area of catalyst.

Sample	Chemical Composition (wt.%)							Si/Al Ratio (mol/mol)	Co/AM * Ratio	SSA ** (m^2/g)
	Si	Al	K	Na	Ca	Fe	Co			
$\text{Al}_2\text{O}_3\text{-Co}$	0.1	49.0	-	0.3	0.1	-	5.2	-	-	212.9

* AM = alkali metals (Na + K), ** SSA = specific surface area (BET).

Table A2. Acidity of cobalt catalyst determined by ammonia TPD.

Sample	c _{SUM} ($\mu\text{mol/g}$)	T _{max1} ($^{\circ}\text{C}$)	c _{max1} ($\mu\text{mol/g}$)	P _{max1} * (%)	T _{max2} ($^{\circ}\text{C}$)	c _{max2} ($\mu\text{mol/g}$)	P _{max2} * (%)	T _{max3} ($^{\circ}\text{C}$)	c _{max3} ($\mu\text{mol/g}$)	P _{max3} * (%)
Al ₂ O ₃ -Co	296	173	178	60	283	118	40	-	-	-

* P = population of the relevant sites, index 1–first deconvolution peak, 2–second deconvolution peak and 3–third deconvolution peak.

Table A3. Basicity of cobalt catalyst determined by CO₂ TPD.

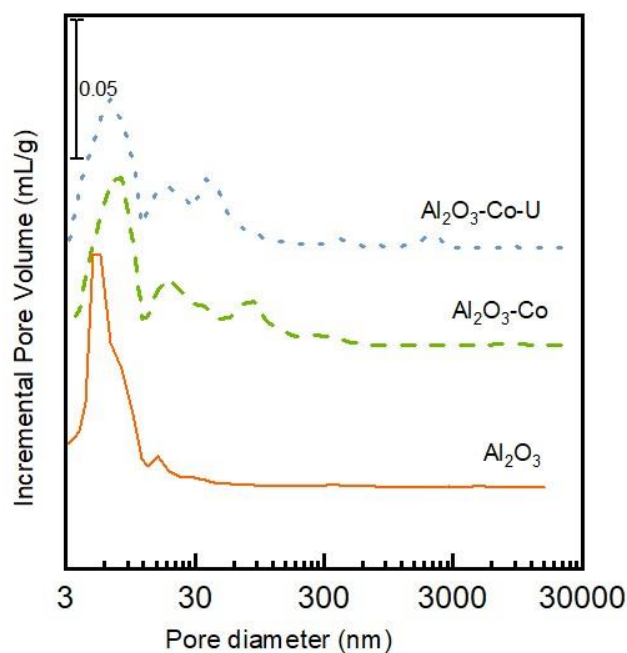
Sample	c _{SUM} ($\mu\text{mol/g}$)	T _{max1} ($^{\circ}\text{C}$)	c _{max1} ($\mu\text{mol/g}$)	P _{max1} * (%)	T _{max2} ($^{\circ}\text{C}$)	c _{max2} ($\mu\text{mol/g}$)	P _{max2} * (%)	T _{max3} ($^{\circ}\text{C}$)	c _{max3} ($\mu\text{mol/g}$)	P _{max3} * (%)
Al ₂ O ₃ -Co	145	109	31	21	144	89	61	263	25	18

* P = population of the relevant sites, index 1–first deconvolution peak, 2–second deconvolution peak and 3–third deconvolution peak.

Table A4. Reducibility of cobalt catalyst determined by TPR.

Sample	c _{SUM} ($\mu\text{mol/g}$)	T _{max1} ($^{\circ}\text{C}$)	c _{max1} ($\mu\text{mol/g}$)	P _{max1} * (%)	T _{max2} ($^{\circ}\text{C}$)	c _{max2} ($\mu\text{mol/g}$)	P _{max2} * (%)	T _{max3} ($^{\circ}\text{C}$)	c _{max3} ($\mu\text{mol/g}$)	P _{max3} * (%)
Al ₂ O ₃ -Co	109	-	-	-	435	85	80	479	24	20

* P = population of the relevant sites, index 1–first deconvolution peak, 2–second deconvolution peak and 3–third deconvolution peak.

**Figure A1.** Pore distribution of Al₂O₃ support, fresh and used cobalt catalyst.

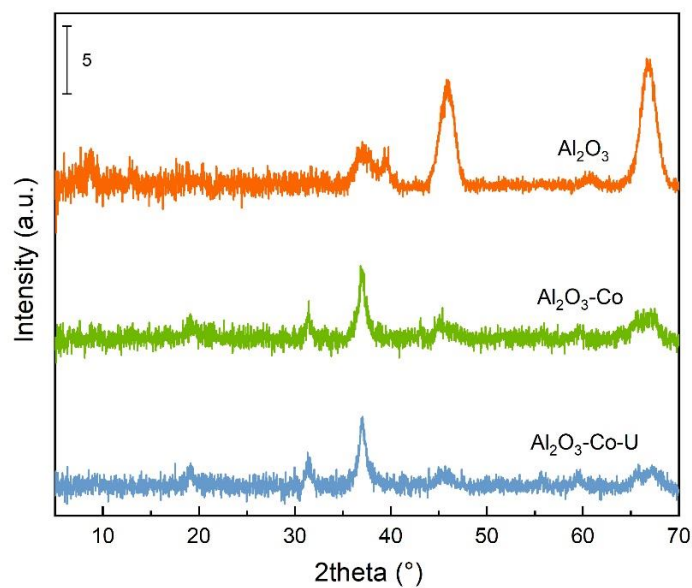


Figure A2. Powder diffraction patterns of Al_2O_3 support, fresh and used cobalt catalyst.

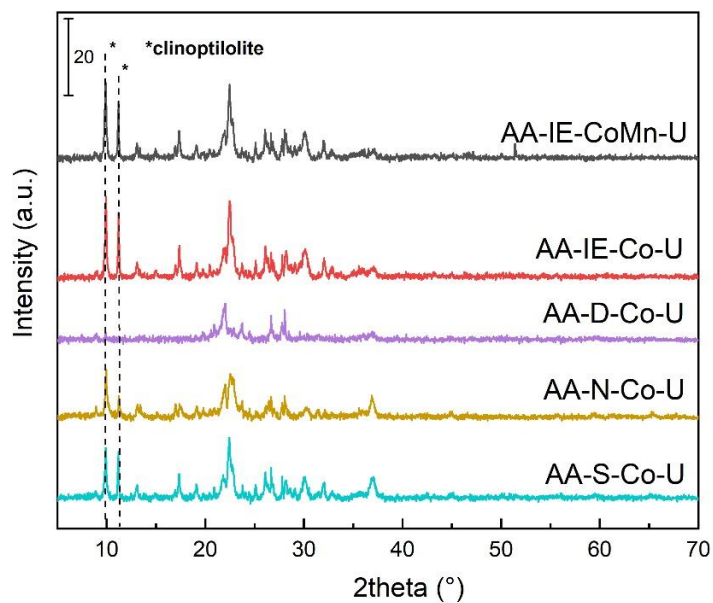


Figure A3. Powder diffraction patterns of used cobalt catalysts.

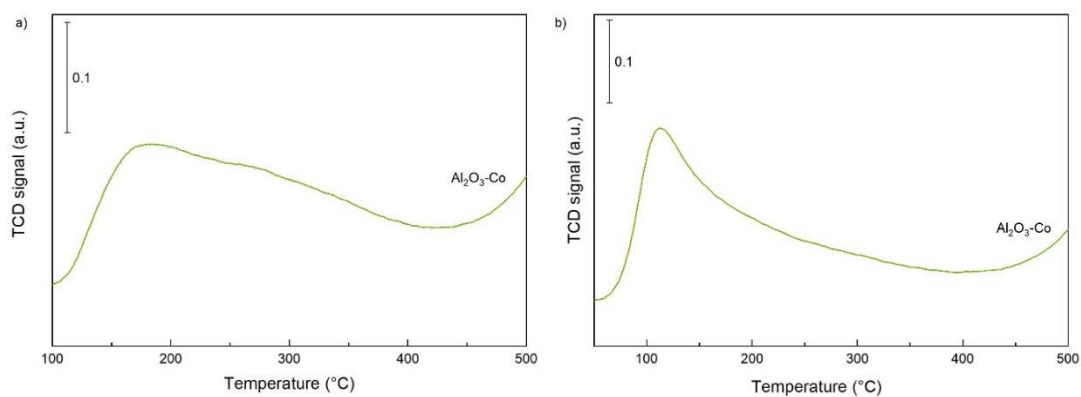


Figure A4. Acidity (a) and basicity (b) of Al_2O_3 cobalt catalyst determined by NH_3 -TPD and CO_2 -TPD, respectively.

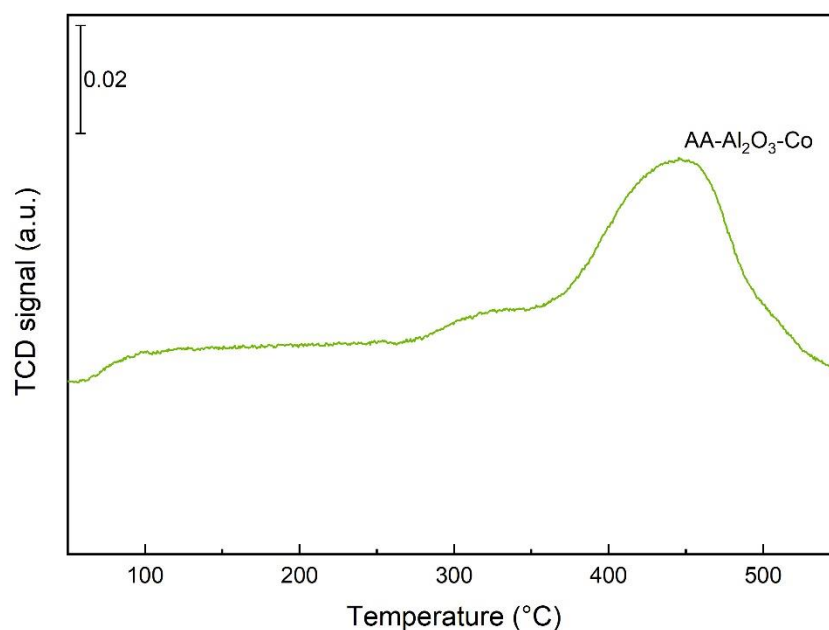


Figure A5. H₂-TPR profiles of Al₂O₃ cobalt catalyst.

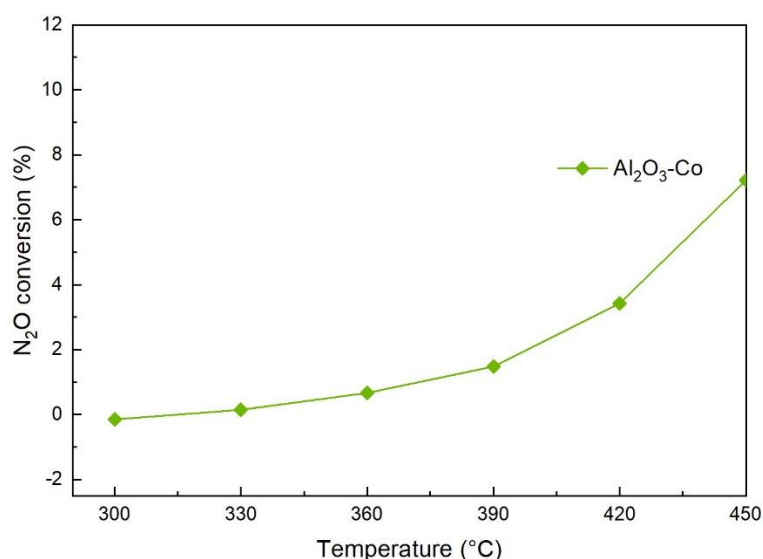


Figure A6. N₂O conversion of Al₂O₃ cobalt catalyst.

References

1. Choya, A.; De Rivas, B.; Gutiérrez-Ortiz, J.I.; Velasco, J.R.G.; López-Fonseca, R. Synthesis, Characterization and Kinetic Behavior of Supported Cobalt Catalysts for Oxidative after-Treatment of Methane Lean Mixtures. *Materials* **2019**, *12*, 3174. [[CrossRef](#)] [[PubMed](#)]
2. Lin, H.-K.; Wang, C.-B.; Chiu, H.-C.; Chien, S.-H. In situ FTIR Study of Cobalt Oxides for the Oxidation of Carbon Monoxide. *Catal. Lett.* **2003**, *86*, 63–68. [[CrossRef](#)]
3. Zhang, J.; Li, Y.; Wang, L.; Zhang, C.; He, H. Catalytic oxidation of formaldehyde over manganese oxides with different crystal structures. *Catal. Sci. Technol.* **2015**, *5*, 2305–2313. [[CrossRef](#)]
4. Hrachovcová, K.; Tišler, Z.; Svobodová, E.; Šafář, J. Modified Alkali Activated Zeolite Foams with Improved Textural and Mechanical Properties. *Minerals* **2020**, *10*, 483. [[CrossRef](#)]
5. Atkins, P.W.; Jones, L.L. *Chemistry: Molecules, Matter, and Change*, 3rd ed.; W. H. Freeman and Company: New York, NY, USA, 1997.

6. Hidalgo-Herrador, J.M.; Tišler, Z.; Vráblík, A.; Velvarská, R.; Lederer, J. Acid-modified phonolite and foamed zeolite as supports for NiW catalysts for deoxygenation of waste rendering fat. *React. Kinet. Mech. Catal.* **2019**, *126*, 773–793. [[CrossRef](#)]
7. Tišler, Z.; Velvarská, R.; Skuhrovcová, L.; Pelišková, L.; Akhmetzyanova, U. Key Role of Precursor Nature in Phase Composition of Supported Molybdenum Carbides and Nitrides. *Materials* **2019**, *12*, 415. [[CrossRef](#)] [[PubMed](#)]
8. Tišler, Z.; Horacek, J.; Safar, J.; Velvarska, R.; Peliskova, L.; Kocik, J.; Gherib, Y.; Marklova, K.; Bulánek, R.; Kubička, D. Clinoptilolite foams prepared by alkali activation of natural zeolite and their post-synthesis modifications. *Microporous Mesoporous Mater.* **2019**, *282*, 169–178. [[CrossRef](#)]
9. Maniak, G.; Stelmachowski, P.; Kotarba, A.; Sojka, Z.; Pérez, V.R.; López, A.B. Rationales for the selection of the best precursor for potassium doping of cobalt spinel based deN₂O catalyst. *Appl. Catal. B Environ.* **2013**, *136*, 302–307. [[CrossRef](#)]
10. Sun, M.; Wang, L.; Feng, B.; Zhang, Z.; Lu, G.; Guo, Y. The role of potassium in K/Co₃O₄ for soot combustion under loose contact. *Catal. Today* **2011**, *175*, 100–105. [[CrossRef](#)]
11. Obalová, L.; Pacultová, K.; Balabánová, J.; Jiráťová, K.; Bastl, Z.; Valášková, M.; Lacný, Z.; Kovanda, F. Effect of Mn/Al ratio in Co–Mn–Al mixed oxide catalysts prepared from hydrotalcite-like precursors on catalytic decomposition of N₂O. *Catal. Today* **2007**, *119*, 233–238. [[CrossRef](#)]
12. Ramírez, J.P.; Kapteijn, F.; Schöffel, K.; Moulijn, J.A. Formation and control of N₂O in nitric acid production: Where do we stand today? *Appl. Catal. B Environ.* **2003**, *44*, 117–151. [[CrossRef](#)]
13. Kapteijn, F.; Marbán, G.; Mirasol, J.R.; Moulijn, J.A. Kinetic Analysis of the Decomposition of Nitrous Oxide over ZSM 5 Catalysts. *J. Catal.* **1997**, *167*, 256–265. [[CrossRef](#)]
14. Asano, K.; Ohnishi, C.; Iwamoto, S.; Shioya, Y.; Inoue, M. Potassium-doped Co₃O₄ catalyst for direct decomposition of N₂O. *Appl. Catal. B Environ.* **2008**, *78*, 242–249. [[CrossRef](#)]
15. Maniak, G.; Stelmachowski, P.; Zasada, F.; Piskorz, W.; Kotarba, A.; Sojka, Z. Guidelines for optimization of catalytic activity of 3d transition metal oxide catalysts in N₂O decomposition by potassium promotion. *Catal. Today* **2011**, *176*, 369–372. [[CrossRef](#)]
16. Maniak, G.; Stelmachowski, P.; Stanek, J.J.; Kotarba, A.; Sojka, Z. Catalytic properties in N₂O decomposition of mixed cobalt–iron spinels. *Catal. Commun.* **2011**, *15*, 127–131. [[CrossRef](#)]
17. Stelmachowski, P.; Maniak, G.; Kotarba, A.; Sojka, Z. Strong electronic promotion of Co₃O₄ towards N₂O decomposition by surface alkali dopants. *Catal. Commun.* **2009**, *10*, 1062–1065. [[CrossRef](#)]
18. Cheng, H.; Huang, Y.; Wang, A.; Li, L.; Wang, X.; Zhang, T. N₂O decomposition over K-promoted Co–Al catalysts prepared from hydrotalcite-like precursors. *Appl. Catal. B Environ.* **2009**, *89*, 391–397. [[CrossRef](#)]
19. Zhang, X.; Shen, Q.; He, C.; Wang, Y.; Cheng, J.; Hao, Z. CoMOR zeolite catalyst prepared by buffered ion exchange for effective decomposition of nitrous oxide. *J. Hazard. Mater.* **2011**, *192*, 1756–1765. [[CrossRef](#)] [[PubMed](#)]
20. Pasha, N.; Lingaiah, N.; Babu, N.S.; Reddy, P.S.S.; Prasad, P.S. Studies on cesium doped cobalt oxide catalysts for direct N₂O decomposition in the presence of oxygen and steam. *Catal. Commun.* **2008**, *10*, 132–136. [[CrossRef](#)]
21. Da Cruz, R.; Mascarenhas, A.; Andrade, H.M.C. Co-ZSM-5 catalysts for N₂O decomposition. *Appl. Catal. B Environ.* **1998**, *18*, 223–231. [[CrossRef](#)]
22. Shen, Q.; Li, L.; Li, J.; Tian, H.; Hao, Z. A study on N₂O catalytic decomposition over Co/MgO catalysts. *J. Hazard. Mater.* **2009**, *163*, 1332–1337. [[CrossRef](#)] [[PubMed](#)]
23. Karásková, K.; Obalová, L.; Jiráťová, K.; Kovanda, F. Effect of promoters in Co–Mn–Al mixed oxide catalyst on N₂O decomposition. *Chem. Eng. J.* **2010**, *160*, 480–487. [[CrossRef](#)]
24. Klyushina, A.; Pacultová, K.; Karásková, K.; Jiráťová, K.; Ritz, M.; Fridrichová, D.; Volodarskaja, A.; Obalová, L. Effect of preparation method on catalytic properties of Co–Mn–Al mixed oxides for N₂O decomposition. *J. Mol. Catal. A Chem.* **2016**, *425*, 237–247. [[CrossRef](#)]
25. Campa, M.C.; Indovina, V.; Pietrogiacomi, D. The dependence of catalytic activity for N₂O decomposition on the exchange extent of cobalt or copper in Na-MOR, H-MOR and Na-MFI. *Appl. Catal. B Environ.* **2009**, *91*, 347–354. [[CrossRef](#)]
26. Fellah, M.F.; Onal, I. N₂O decomposition on Fe- and Co-ZSM-5: A density functional study. *Catal. Today* **2008**, *137*, 410–417. [[CrossRef](#)]

27. Obalová, L.; Karásková, K.; Jiráťová, K.; Kovanda, F. Effect of potassium in calcined Co–Mn–Al layered double hydroxide on the catalytic decomposition of N₂O. *Appl. Catal. B Environ.* **2009**, *90*, 132–140. [[CrossRef](#)]
28. Stelmachowski, P.; Ciura, K.; Grzybek, G. Morphology-dependent reactivity of cobalt oxide nanoparticles in N₂O decomposition. *Catal. Sci. Technol.* **2016**, *6*, 5554–5560. [[CrossRef](#)]
29. Gudyka, S.; Grzybek, G.; Gryboś, J.; Indyka, P.; Leszczyński, B.; Kotarba, A.; Sojka, Z. Enhancing the deN₂O activity of the supported Co₃O₄/α-Al₂O₃ catalyst by glycerol-assisted shape engineering of the active phase at the nanoscale. *Appl. Catal. B Environ.* **2017**, *201*, 339–347. [[CrossRef](#)]
30. Grzybek, G.; Wójcik, S.; Legutko, P.; Gryboś, J.; Indyka, P.; Leszczyński, B.; Kotarba, A.; Sojka, Z. Thermal stability and repartition of potassium promoter between the support and active phase in the K Co_{2.6}Zn_{0.4}O₄/α-Al₂O₃ catalyst for N₂O decomposition: Crucial role of activation temperature on catalytic performance. *Appl. Catal. B Environ.* **2017**, *205*, 597–604. [[CrossRef](#)]
31. Boroń, P.; Chmielarz, L.; Casale, S.; Calers, C.; Krafft, J.-M.; Dzwigaj, S. Effect of Co content on the catalytic activity of CoSiBEA zeolites in N₂O decomposition and SCR of NO with ammonia. *Catal. Today* **2015**, *258*, 507–517. [[CrossRef](#)]
32. Liu, N.; Zhang, R.; Chen, B.; Li, Y.; Li, Y. Comparative study on the direct decomposition of nitrous oxide over M (Fe, Co, Cu)–BEA zeolites. *J. Catal.* **2012**, *294*, 99–112. [[CrossRef](#)]
33. Smeets, P.J.; Meng, Q.; Corthals, S.; Leeman, H.; Schoonheydt, R.A. Co–ZSM-5 catalysts in the decomposition of N₂O and the SCR of NO with CH₄: Influence of preparation method and cobalt loading. *Appl. Catal. B Environ.* **2008**, *84*, 505–513. [[CrossRef](#)]
34. Ghahri, A.; Golbabaie, F.; Vafajoo, L.; Mireskandari, S.M.; Yaseri, M.; Shahtaheri, S.J. Removal of Greenhouse Gas (N₂O) by Catalytic Decomposition on Natural Clinoptilolite Zeolites Impregnated with Cobalt. *Int. J. Environ. Res.* **2017**, *11*, 327–337. [[CrossRef](#)]
35. Obalová, L.; Karásková, K.; Wach, A.; Kustrowski, P.; Kutlákova, K.M.; Michalik, S.; Jiráťová, K. Alkali metals as promoters in Co–Mn–Al mixed oxide for N₂O decomposition. *Appl. Catal. A Gen.* **2013**, *462–463*, 227–235. [[CrossRef](#)]
36. Abu-Zied, B.M.; Soliman, S.A.; Abdellah, S.E. Pure and Ni-substituted Co₃O₄ spinel catalysts for direct N₂O decomposition. *Chin. J. Catal.* **2014**, *35*, 1105–1112. [[CrossRef](#)]
37. Del Río, L.; Marbán, G. Stainless steel wire mesh supported potassium doped cobalt oxide catalysts for the catalytic decomposition of nitrous oxide. *Appl. Catal. B Environ.* **2012**, *126*, 39–46. [[CrossRef](#)]
38. Karásková, K.; Obalová, L.; Kovanda, F. N₂O catalytic decomposition and temperature programmed desorption tests on alkali metals promoted Co–Mn–Al mixed oxide. *Catal. Today* **2011**, *176*, 208–211. [[CrossRef](#)]
39. Žaneta, C.; Obalová, L.; Kovanda, F.; Legut, D.; Titov, A.; Ritz, M.; Fridrichová, D.; Michalik, S.; Kuśtrowski, P.; Jiráťová, K. Effect of precursor synthesis on catalytic activity of Co₃O₄ in N₂O decomposition. *Catal. Today* **2015**, *257*, 18–25. [[CrossRef](#)]
40. Xue, L.; Zhang, C.; He, H.; Teraoka, Y. Catalytic decomposition of N₂O over CeO₂ promoted Co₃O₄ spinel catalyst. *Appl. Catal. B Environ.* **2007**, *75*, 167–174. [[CrossRef](#)]
41. Piskorz, W.; Zasada, F.; Stelmachowski, P.; Kotarba, A.; Sojka, Z. Decomposition of N₂O over the surface of cobalt spinel: A DFT account of reactivity experiments. *Catal. Today* **2008**, *137*, 418–422. [[CrossRef](#)]
42. Xue, L.; Zhang, C.; He, H.; Teraoka, Y. Promotion effect of residual K on the decomposition of N₂O over cobalt–cerium mixed oxide catalyst. *Catal. Today* **2007**, *126*, 449–455. [[CrossRef](#)]
43. Klegova, A.; Inayat, A.; Indyka, P.; Gryboś, J.; Sojka, Z.; Pacultová, K.; Schwieger, W.; Volodarskaja, A.; Kuśtrowski, P.; Rokicińska, A.; et al. Cobalt mixed oxides deposited on the SiC open-cell foams for nitrous oxide decomposition. *Appl. Catal. B Environ.* **2019**, *255*, 255. [[CrossRef](#)]
44. Iwanek, E.; Krawczyk, K.; Petryk, J.; Sobczak, J.W.; Kaszkur, Z. Direct nitrous oxide decomposition with CoOx/CeO₂ catalysts. *Appl. Catal. B Environ.* **2011**, *106*, 416–422. [[CrossRef](#)]
45. Thangavelu, K.; Parameswari, K.; Kuppusamy, K.; Haldorai, Y. A simple and facile method to synthesize Co₃O₄ nanoparticles from metal benzoate dihydrazinate complex as a precursor. *Mater. Lett.* **2011**, *65*, 1482–1484. [[CrossRef](#)]
46. Russo, N.; Fino, D.; Saracco, G.; Specchia, V. N₂O catalytic decomposition over various spinel-type oxides. *Catal. Today* **2007**, *119*, 228–232. [[CrossRef](#)]

47. Grzybek, G.; Stelmachowski, P.; Indyka, P.; Inger, M.; Wilk, M.; Kotarba, A.; Sojka, Z. Cobalt–zinc spinel dispersed over cordierite monoliths for catalytic N₂O abatement from nitric acid plants. *Catal. Today* **2015**, *257*, 93–97. [[CrossRef](#)]
48. Zhang, R.; Hedjazi, K.; Chen, B.; Li, Y.; Lei, Z.; Liu, N. M(Fe, Co)-BEA washcoated honeycomb cordierite for N₂O direct decomposition. *Catal. Today* **2016**, *273*, 273–285. [[CrossRef](#)]
49. JirátoVá, K.; Balabánová, J.; Kovanda, F.; Klegová, A.; Obalová, L.; Fajgar, R. Cobalt Oxides Supported Over Ceria–Zirconia Coated Cordierite Monoliths as Catalysts for Deep Oxidation of Ethanol and N₂O Decomposition. *Catal. Lett.* **2017**, *147*, 1379–1391. [[CrossRef](#)]
50. Klyushina, A.; Pacultová, K.; Krejčová, S.; Słowik, G.; JirátoVá, K.; Kovanda, F.; Ryczkowski, J.; Obalová, L. Advantages of stainless steel sieves as support for catalytic N₂O decomposition over K doped Co₃O₄. *Catal. Today* **2015**, *257 Pt 1*, 2–10. [[CrossRef](#)]
51. Klegová, A.; Pacultová, K.; Fridrichová, D.; Volodarskaja, A.; Kovanda, F.; JirátoVá, K. Cobalt Oxide Catalysts on Commercial Supports for N₂O Decomposition. *Chem. Eng. Technol.* **2017**, *40*, 981–990. [[CrossRef](#)]
52. Pacultová, K.; Klegova, A.; Kiška, T.; Fridrichová, D.; Martaus, A.; Rokicińska, A.; Kuśtrowski, P.; Obalová, L. Effect of support on the catalytic activity of Co₃O₄-Cs deposited on open-cell ceramic foams for N₂O decomposition. *Mater. Res. Bull.* **2020**, *129*, 110892. [[CrossRef](#)]
53. Rutkowska, M.; Piwowarska, Z.; Micek, E.; Chmielarz, L. Hierarchical Fe-, Cu- and Co-Beta zeolites obtained by mesotemplate-free method. Part I: Synthesis and catalytic activity in N₂O decomposition. *Microporous Mesoporous Mater.* **2015**, *209*, 54–65. [[CrossRef](#)]
54. Sadek, R.; Chalupka, K.A.; Mierczynski, P.; Rynkowski, J.; Gurgul, J.; Dzwigaj, S. Cobalt Based Catalysts Supported on Two Kinds of Beta Zeolite for Application in Fischer-Tropsch Synthesis. *Catalysts* **2019**, *9*, 497. [[CrossRef](#)]
55. Kang, S.-H.; Ryu, J.-H.; Kim, J.-H.; Jang, I.H.; Kim, A.R.; Han, G.Y.; Bae, J.W.; Ha, K.-S. Role of ZSM5 Distribution on Co/SiO₂ Fischer–Tropsch Catalyst for the Production of C₅–C₂₂ Hydrocarbons. *Energy Fuels* **2012**, *26*, 6061–6069. [[CrossRef](#)]
56. Kurian, M.; Thankachan, S.; Nair, D.S.; Aswathy, E.K.; Babu, A.; Thomas, A.; KT, B.K. Structural, magnetic, and acidic properties of cobalt ferrite nanoparticles synthesised by wet chemical methods. *J. Adv. Ceram.* **2015**, *4*, 199–205. [[CrossRef](#)]

Publisher’s Note: MDPI stays neutral with regard to jurisdictional claims in published maps and institutional affiliations.



© 2020 by the authors. Licensee MDPI, Basel, Switzerland. This article is an open access article distributed under the terms and conditions of the Creative Commons Attribution (CC BY) license (<http://creativecommons.org/licenses/by/4.0/>).